Supplementary Information

Two-photon all-optical neurophysiology for the dissection of larval zebrafish brain functional and effective connectivity

Lapo Turrini[1,2,3,*], Pietro Ricci[3,4], Michele Sorelli[2,3], Giuseppe de Vito[1,2,5], Marco Marchetti[6], Francesco Vanzi[2,7], Francesco S. Pavone[1,2,3,*]

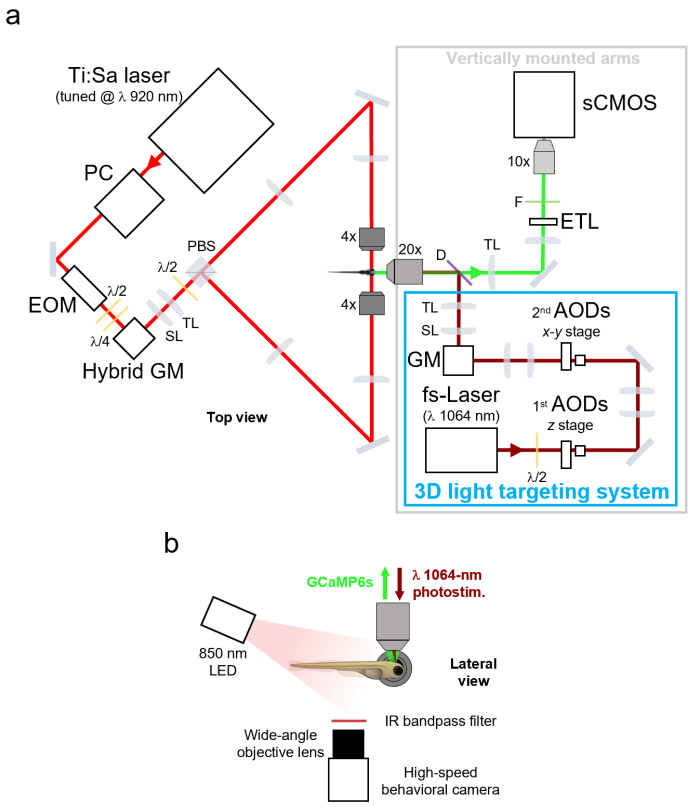

Supplementary Figure 1. Scheme of the optical setup.
a. Schematic representation (top view) of the optical setup devised for simultaneous whole-brain imaging and optogenetic stimulation. Red line indicates the 920 nm excitation path employed for light-sheet imaging, green indicates GCaMP6s fluorescence in the imaging detection path, darker red indicates the 1064 nm excitation of the 3D light-targeting system used for stimulation. Arrows at the beginning of each optical path indicate the direction of light propagation. PC, pulse compressor; EOM, electro-optical modulator; λ/2, half-wave plate; λ/4, quarter-wave plate; GM, galvo mirrors; SL, scan lens; TL, tube lens; PBS, polarizing beam splitter; D, dichroic mirror; ETL, electrically tunable lens; F, fluorescence filter; AODs, acousto-optic deflectors. See Optical setup for details. **b.** Schematic representation of the behavioral imaging components employed for tail tracking during whole-brain functional imaging. The lateral view of a zebrafish larva inside the imaging chamber (not represented, for clarity purpose) is depicted. An 850 nm LED is used to provide illumination for behavioral imaging. A high-speed camera coupled to a wide-angle objective lens is placed beneath the transparent PMMA bottom of the imaging chamber. Light coming from the NIR LED is selected through a NIR bandpass filter. The second illumination objective for light-sheet excitation is not displayed.

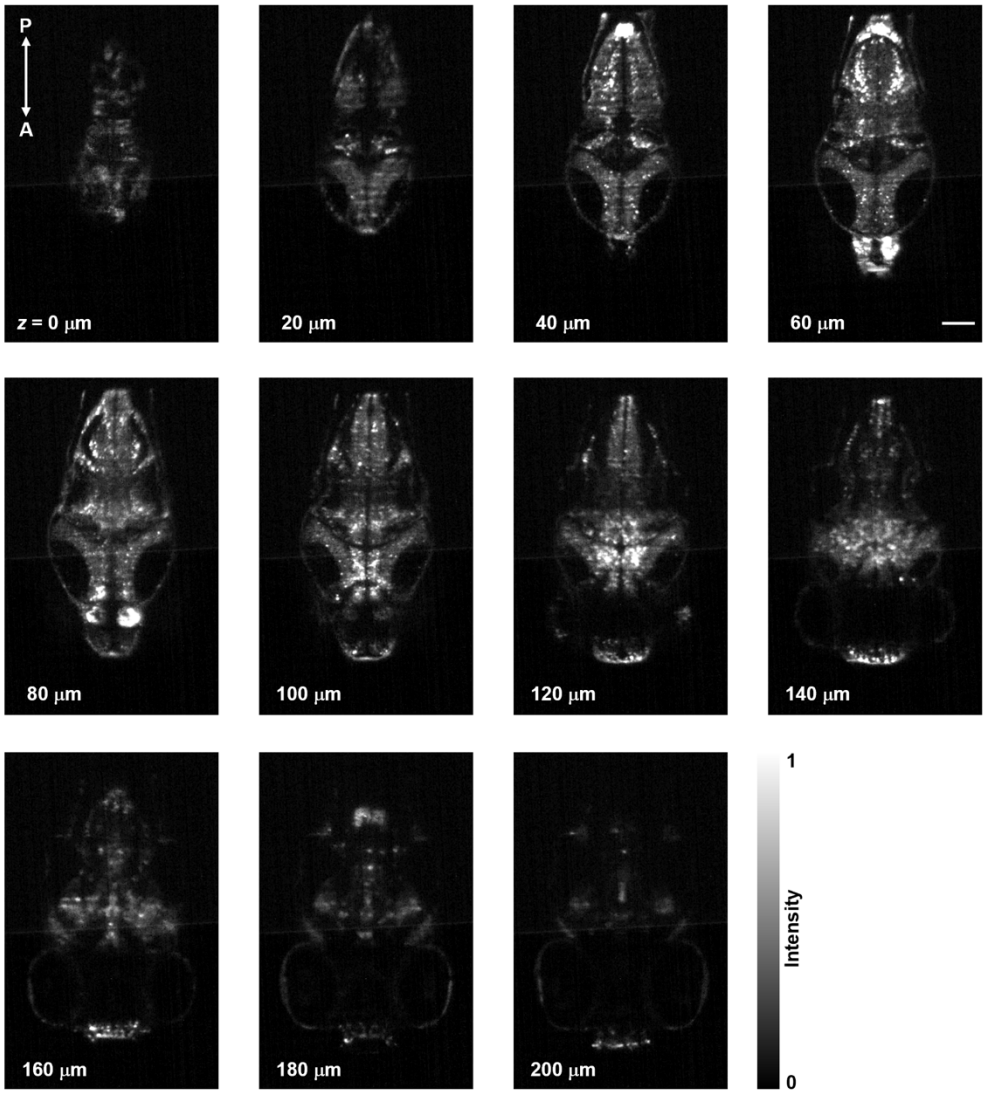

Supplementary Figure 2. Larval zebrafish brain planes sampled at different depths.
Brain planes of one representative 5 dpf *Tg(elavl3:H2B-GCaMP6; elavl3:ReaChR-TagRFP)* larval zebrafish imaged with 2P LSFM. Imaging was performed over a brain depth of 200 μm with a step size of 5 μm (see also Supplementary Movie 1). Depth from the surface is indicated on each image. Images are time average projections of each plane over a time window of 30 s. Gray levels show fluorescence signal arising from the GCaMP6s calcium sensor. Dim red fluorescence signal from TagRFP excited at 920 nm was filtered out before reaching the sensor (see Optical setup for details).
Scale bar, 100 μm. A, anterior; P, posterior.

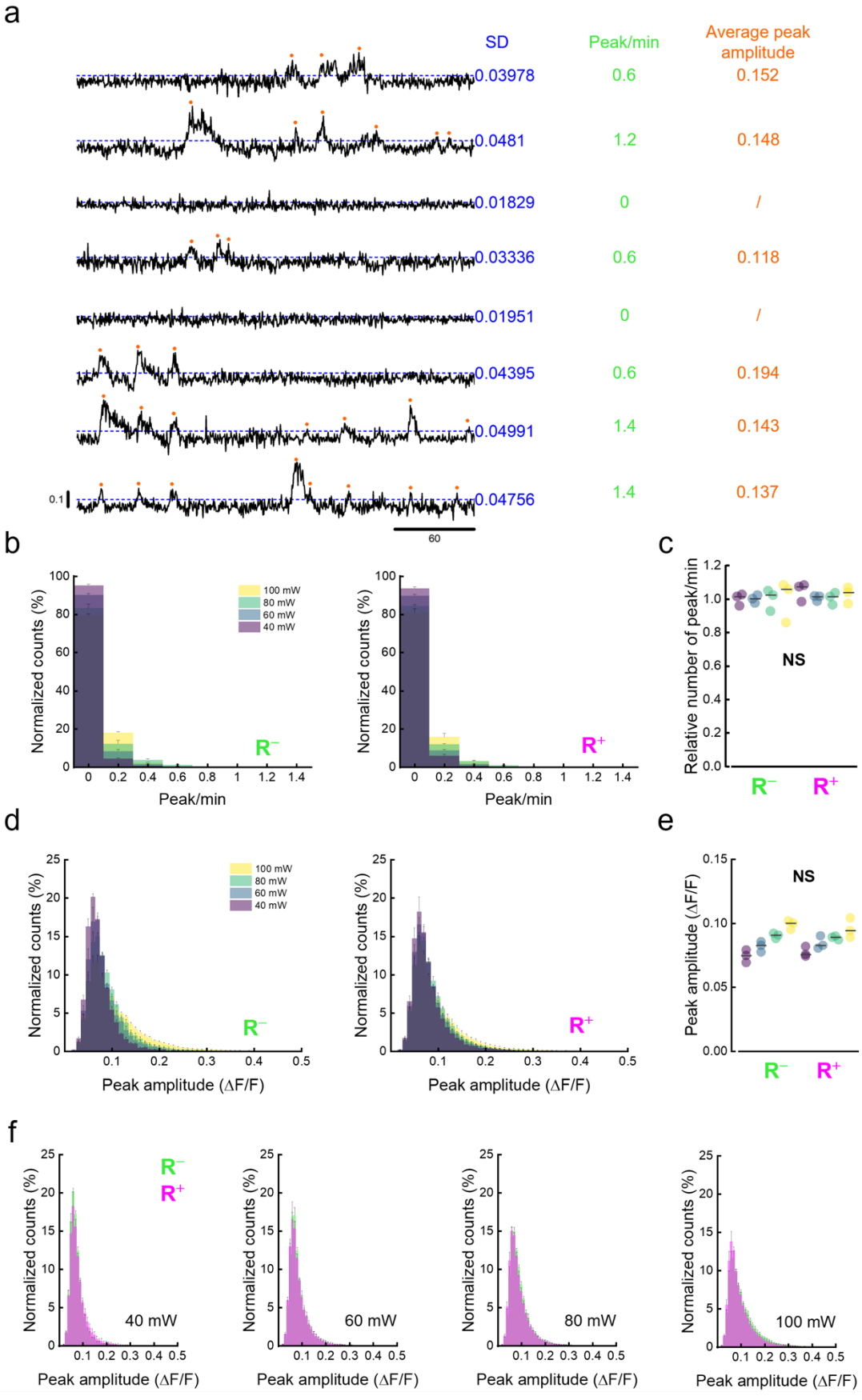
a
SD
Peak/min
Average peak amplitude
0.03978
0.6
0.152
0.0481
1.2
0.148
0.01829
0
/
0.03336
0.6
0.118
0.01951
0
/
0.04395
0.6
0.194
0.04991
1.4
0.143
0.04756
1.4
0.137
0.1
60
b
Normalized counts (%)
100 mW
80 mW
60 mW
40 mW
R⁻
R⁺
Peak/min
c
Relative number of peak/min
NS
R⁻
R⁺
d
Normalized counts (%)
Peak amplitude (ΔF/F)
e
Peak amplitude (ΔF/F)
NS
f
40 mW
60 mW
80 mW
100 mW

Supplementary Figure 3. Comparison of different metrics for the quantification of neuronal activity levels.

a. Representative time traces of 18 voxels sampled from the brain a *Tg(elavl3:H2B-GCaMP6; elavl3:ReaChR-TagRFP)* larva during 5 minutes of whole-brain calcium imaging (volumetric rate: 2.5 Hz, λ_{ex}: 920 nm, power: 60 mW). The three different metrics we considered are: the standard deviation (SD) over time (blue), the average number of peaks per minute (green), and the average peak amplitude (orange). Blue dashed lines indicate the SD values reported on the right of the traces. Orange dots represent events that were automatically identified as calcium peaks according to the constraints imposed (see *Data analysis* for details). Scale bars: horizontal, s; vertical, $\Delta F/F$. **b.** Average normalized distributions of the peak/min values of voxels composing the larval brain over 5 minutes of continuous light-sheet imaging at increasing laser power (40, 60, 80 and 100 mW) for ReaChR$^-$ (R^-) and ReaChR$^+$ (R^+) larvae. **c.** Relative number of peak/min for ReaChR$^+$ and ReaChR$^-$larvae. Each data point is obtained by subtracting the average peak/min of ReaChR$^-$ larvae from the individual value of each larva. No statistically significant difference is observable neither between zebrafish strains nor between imaging powers. **d.** Average normalized distributions of the average peak amplitude values of voxels composing the larval brain over 5 minutes of continuous light-sheet imaging at increasing laser power (40, 60, 80 and 100 mW) for ReaChR$^-$ and ReaChR$^+$ larvae. **e.** Median peak amplitude values calculated from individual peak amplitude distributions of brain-wide voxels of ReaChR$^-$ and ReaChR$^+$ larvae. Statistical comparisons (two-way ANOVA and post-hoc Tukey's test) highlight no statistical significance ($P>0.05$) between peak amplitude values of ReaChR$^-$ and ReaChR$^+$ larvae exposed to the same imaging power. **f.** Average normalized distributions of the average peak amplitude values of larval brain voxels over 5 minutes of continuous light-sheet imaging at laser powers of 40, 60, 80 and 100 mW for ReaChR$^+$ and ReaChR$^-$ larvae. N = 3 ReaChR$^-$ and 3 ReaChR$^+$. Error bars of average distributions in panels b, d and f indicate the sem. Color code of data points in panels c and e is the same as in panel b. Gray horizontal bars in panels c and e represent intragroup mean values.

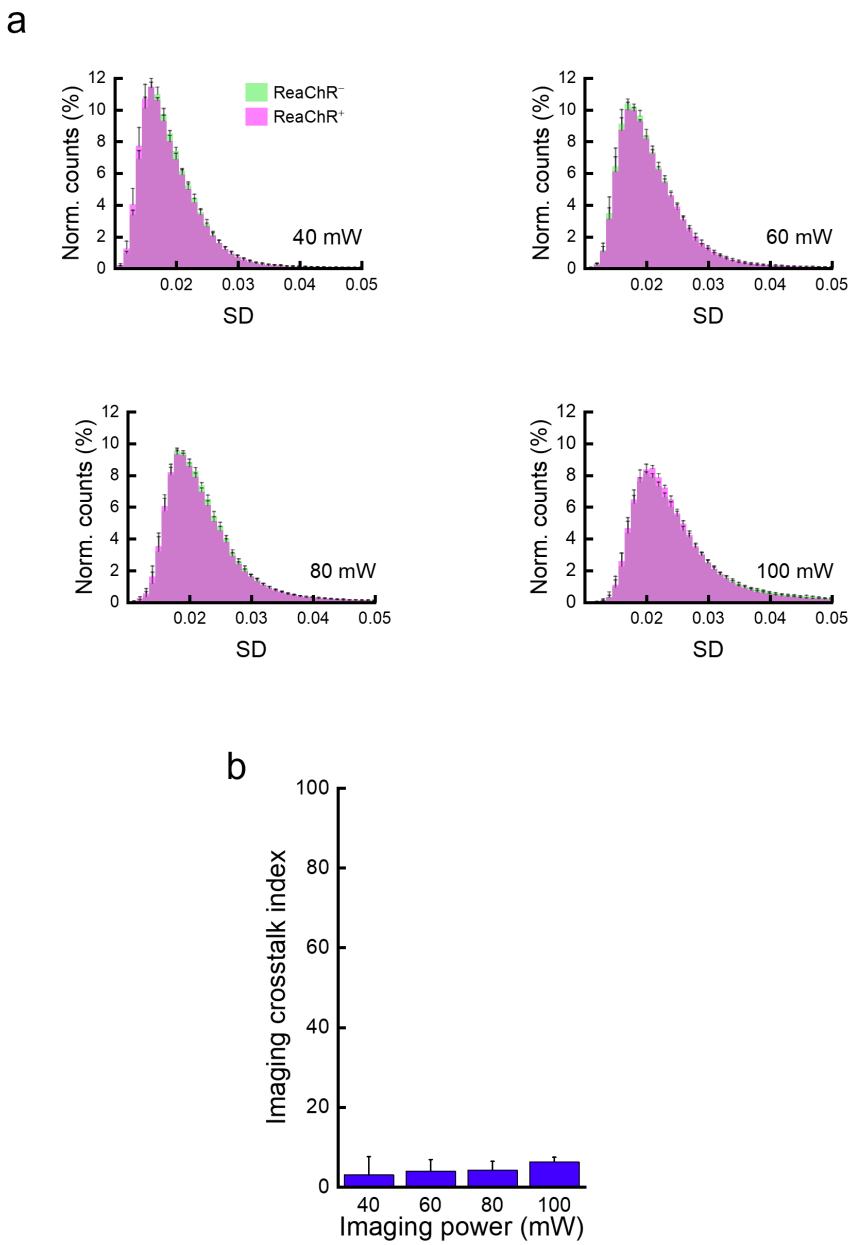

Supplementary Figure 4. Neuronal activity levels at increasing imaging power.
a. Average normalized distributions of the SD values of larval brain voxels over 5 minutes of continuous light-sheet imaging (volumetric rate: 2.5 Hz, λ_{ex}: 920 nm) at laser powers of 40, 60, 80 and 100 mW for ReaChR$^+$ and ReaChR$^-$ larvae. N = 3 ReaChR$^+$ and 3 ReaChR$^-$ larvae. **b.** Imaging crosstalk index (Hellinger distance between ReaChR$^+$ and ReaChR$^-$ distributions) computed for the different power levels tested. Error bars were calculated according to uncertainty propagation theory (see Data analysis for details).

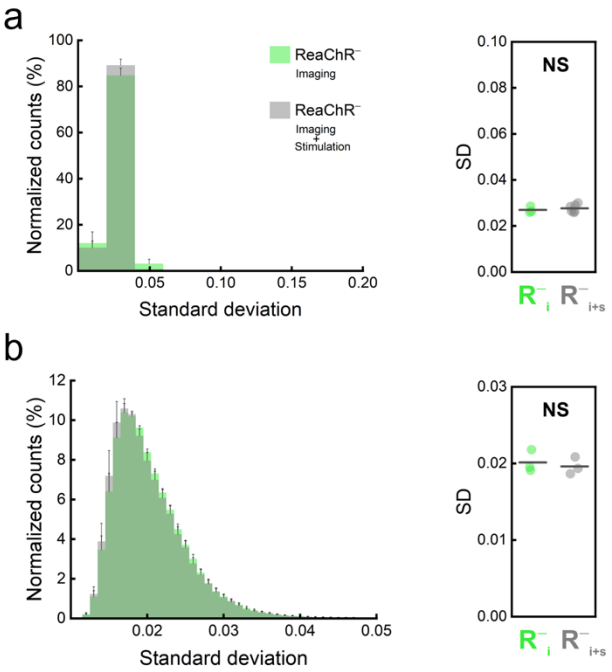

Supplementary Figure 5. Specificity of the optogenetic stimulation.
a. Left, average normalized distributions of SD values inside the stimulation site of ReaChR⁻ larvae exposed to imaging only (green) or to imaging and photostimulation (gray). **Right,** comparison of median SD values calculated from individual SD distributions at the stimulation site of ReaChR⁻ larvae undergoing imaging (R^-_i) or both imaging and stimulation (R^-_{i+s}). Intergroup comparisons highlight no statistical significance. NS P = 0.5584, unpaired t test. **b. Left,** average normalized distributions of the SD values of voxels composing the brain of ReaChR⁻ larvae exposed to imaging only (green) or to imaging and photostimulation (gray). **Right,** comparison of median SD values calculated from individual brain-wide SD distributions of ReaChR⁻ larvae during imaging or imaging and stimulation. Intergroup comparisons highlight no statistically significant difference. NS P = 0.6510, unpaired t test.

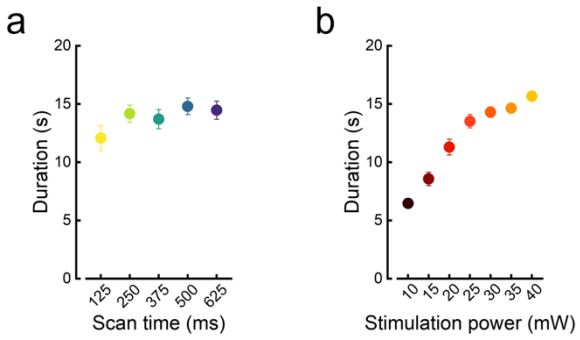

Supplementary Figure 6. Duration of calcium transients evoked by photostimulation.
Average duration of calcium transients as a function of scan time (**a**) and stimulation power (**b**). Symbols are color coded as in Figure 2. Data are presented as mean ± sem. Where not visible, error bars are smaller than symbol size. N = 4 ReaChR^{+} larvae, n = 3 calcium transients per larva.

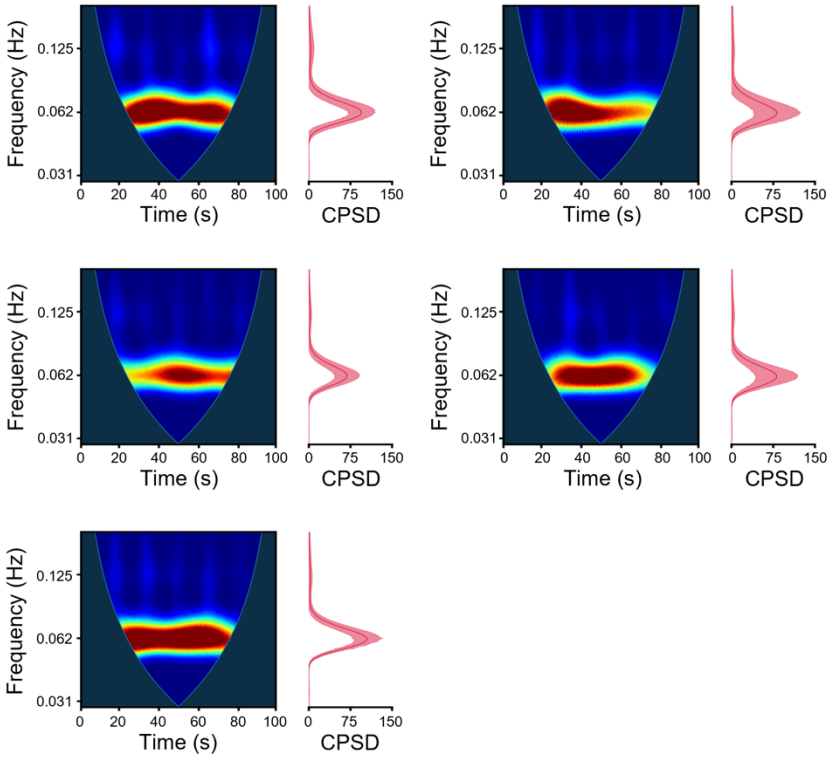

Supplementary Figure 7. Cross power spectrum of left habenula and IPN activity for different larvae. Cross-wavelet power spectral density (CPSD) between the LHb and IPN time traces (one trial for each of the tested larvae). Warmer colors indicate higher power density levels. On the right of each spectrum is a plot showing the time-averaged CPSD with 95% confidence intervals: a high level of interindividual consistency is observed. N = 5 ReaChR^{+} larvae.

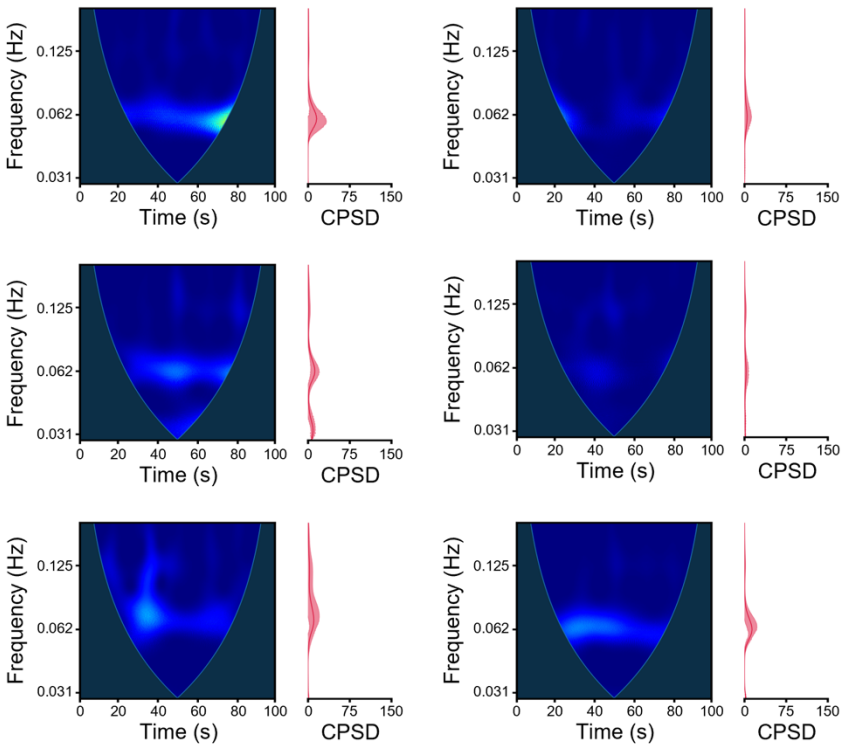

Supplementary Figure 8. Cross power spectrum of left and right habenula activity for different larvae. Cross-wavelet power spectra of LHb and RHb time traces (one trial for each of the tested larvae). Warmer colors indicate higher cross-wavelet power spectral density (CPSD). On the right of each spectrum is a plot showing the CPSD averaged over time. Only faint CPSD levels are observed, meaning that the two regions do not share significant frequency components. N = 6 ReaChR^{+} larvae.

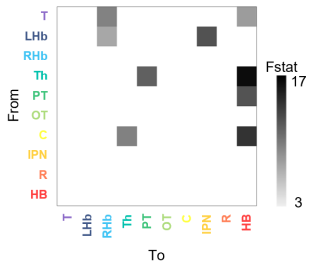

Supplementary Figure 9. Thresholded average causality matrix
Matrix showing the average F statistic values of comparisons having at least 33% of trials with significant causality. The color of each square was employed to display the F statistic magnitude in the arrows presented in Figure 4d (see Supplementary Data 2 for F values).

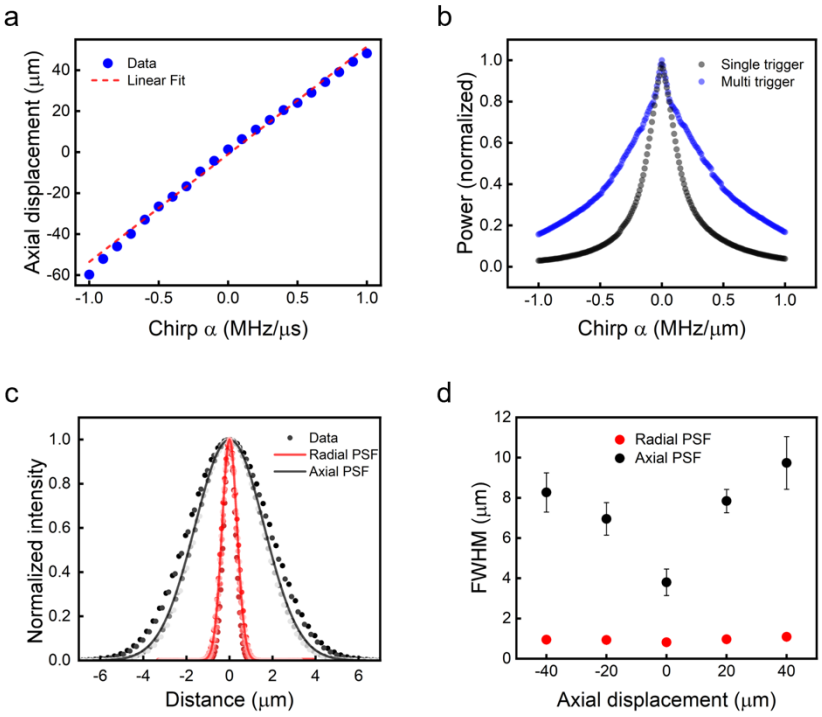

Supplementary Figure 10. Optical characterization of the light-targeting path
a. Axial displacement of the focal point as a function of the chirped frequency applied to AODs. R^2 = 0.99385. Data are presented as mean ± sem. **b.** Normalized laser power as a function of the chirp parameter. In our system, the -1/1 MHz/μs chirp range corresponds to a defocusing range of 100 μm. **c.** System point spread function (PSF) is represented as the normalized intensity of subdiffraction-sized fluorescent beads as a function of the distance from the center of the bead. Results from 5 beads are displayed. Gaussian fits are calculated on N = 25 fluorescent beads. **d.** FWHM of the PSF as a function of the axial displacement (80 μm range) from the native focal plane. Data are presented as mean ± sem. N = 25 fluorescent beads.
Where not visible, error bars are smaller than symbol size.

a

Shapiro-Wilk Normality Test
Activation probability

Region	DF	Statistic	p-value	Decision at level(5%)
T	6	0.94285	0.6822	Can't reject normality
LHb	6	0.83458	0.11749	Can't reject normality
RHb	6	0.91638	0.47968	Can't reject normality
Th	6	0.915	0.47011	Can't reject normality
PT	6	0.97861	0.94443	Can't reject normality
OT	6	0.98014	0.95226	Can't reject normality
C	6	0.88827	0.30923	Can't reject normality
IPN	6	0.9661	0.86529	Can't reject normality
R	6	0.94143	0.6707	Can't reject normality
HB	6	0.9495	0.73626	Can't reject normality

b

Shapiro-Wilk Normality Test
Pearson's correlation coefficient

Region	DF	Statistic	p-value	Decision at level(5%)
T	6	0.95875	0.81004	Can't reject normality
LHb	6	0.81943	0.08725	Can't reject normality
RHb	6	0.82111	0.09023	Can't reject normality
Th	6	0.79901	0.05758	Can't reject normality
PT	6	0.87138	0.23177	Can't reject normality
OT	6	0.8934	0.33637	Can't reject normality
C	6	0.95839	0.80723	Can't reject normality
IPN	6	0.85625	0.17668	Can't reject normality
R	6	0.92081	0.51123	Can't reject normality
HB	6	0.87182	0.23355	Can't reject normality

Supplementary Figure 11. Normality tests
Shapiro-Wilk normality tests for activation probability (**a**) and Pearson's correlation coefficients (**b**)in different brain regions of N = 6 ReaChR^{+} larvae. Results of the tests in both cases accept the null hypothesis that data were drawn from a normally distributed population.

Supplementary Movies legends

Supplementary Movie 1. Larval zebrafish brain imaging with 2P LSFM
Representative light-sheet image stack of the brain of a 5 dpf *Tg(elavl3:H2B-GCaMP6; elavl3:ReaChR-TagRFP)* zebrafish larva. Each plane was time averaged over a window of 30 s to enhance image visibility. Sampled depth, 200 μm with a *z*-step of 5 μm. Movie is played at 2.5 Hz volumetric rate, the same frequency used for imaging. Scale bar, 100 μm.

Supplementary Movie 2. Expression patterns of the double transgenic *Tg(elavl3:H2B-GCaMP6; elavl3:ReaChR-TagRFP) zebrafish line* .
Confocal image stack (z-step: 2 μm) of the head of a 5 dpf *Tg(elavl3:H2B-GCaMP6; elavl3:ReaChR-TagRFP)* zebrafish larva. In green, the nuclear localized fluorescent calcium indicator GCaMP6s. In magenta, the membrane light-gated cation channel ReaChR (expressed as a fusion protein with TagRFP). The *elavl3* promoter drives the expression of both indicator and opsin in all differentiated neurons. Scale bar, 100 μm.

Supplementary Movie 3. ReaChR^{-} larval zebrafish in tail-free preparation during whole-brain imaging OFF and ON.
Representative high-speed (300 Hz) footage of a 5 dpf *Tg(elavl3:H2B-GCaMP6)* zebrafish larva with agarose-restrained head and tail free. The first and the second halves of the video were in absence (OFF) and in presence (ON) of whole-brain imaging, respectively. Larva performs tail beats in both conditions (imaging OFF and ON). Signs of struggle are to be attributed to the fact the larva was not acclimated to the agarose-restrained condition before starting measurements. Beyond the larva, out of focus, it is visible the front pupil of the detection objective used for GCaMP6s fluorescence collection.
Movie is played at 1× speed. Scale bar, 1 mm.

Supplementary Movie 4. ReaChR^{+} larval zebrafish in tail-free preparation during whole-brain imaging OFF and ON.
Representative high-speed (300 Hz) footage of a 5 dpf *Tg(elavl3:H2B-GCaMP6; elavl3:ReaChR-TagRFP)* zebrafish larva with agarose-restrained head and tail free. As in Supplementary Movie 3, the first and the second halves of the video were in absence (OFF) and in presence (ON) of whole-brain imaging, respectively. Larva performs tail beats in both conditions (imaging OFF and ON). Signs of struggle are to be attributed to the fact the larva was not acclimated to the agarose-restrained condition before starting measurements. Beyond the larva, out of focus, it is visible the front pupil of the detection objective used for GCaMP6s fluorescence collection.
Movie is played at 1× speed. Scale bar, 1 mm.

Supplementary Movie 5. Raw timelapse acquisition of whole-brain imaging during optogenetic stimulation of the left habenula.
Composite showing the raw timelapse of 8 evenly distributed *z*-planes of the larval zebrafish brain during a photostimulation trial. Plane depth reported in orange is expressed in μm from the surface of the brain. Stimulation events are indicated by the red dot on the right. Arrowheads indicate the stimulation site (left habenula, blue) and the deep midbrain interpeduncular nucleus (IPN, yellow), described in further analyses. Due to the nuclear localization of the calcium indicator and the specific habenular structure (a dome of neuronal bodies surmounting neuronal processes), left habenula in the plane at 90 μm depth appears as an active fluorescent rim (neuronal nuclei) with dark inner (neuronal processes).
Movie is played at 10× speed. Scale bar, 200 μm.

Supplementary Movie 6. 3D rotation of whole-brain activation probability map in response to left habenula stimulation.
The rotating map shows the average probability of each voxel composing the larval brain to be active as a consequence of optogenetic stimulation of the left habenula. Probability is color mapped as in the color bar (black = 0, white = 1). Map rotates along the larval antero-posterior axis. N = 6 ReaChR^{+} larvae.

Supplementary Movie 7. Volumetric activation probability maps of individual larvae in response to left habenula stimulation.
Composite showing volumetric activation probability maps of individual larvae. Probability is color-mapped as in the color bar. Each map was obtained calculating the probability of activation on n = 30 photostimulation events.

Supplementary Movie 8. Volumetric correlation maps of individual larvae.
Composite of volumetric maps of individual larvae showing the grade of correlation with the optogenetically-induced activity of the left habenula (seed). Pearson's correlation coefficient is color-mapped as in the color bar. Each map was obtained calculating the correlation with the seed over n = 30 photostimulation events.

Supplementary Movie 9. 3D rotation of whole-brain functional connectivity of the left habenula.
The rotating map shows the binarized functional connectivity map of the left habenular nucleus (magenta) overlaid to the brain structure (gray). The map was obtained by binarizing the average seed-based correlation map shown in Figure 4e (Pearson's correlation coefficient threshold: 0.12, as the highest value separating significant from non-significant correlation among brain regions, see light-gray horizontal dotted line in Figure 4f). Map rotates along the larval antero-posterior axis. N = 6 ReaChR^{+} larvae.